Spectroscopic Properties of the Carotenoid 3′-Hydroxyechinenone in the Orange Carotenoid Protein from the Cyanobacterium *Arthrospira maxima*†

Tomáš Polívka,*,‡ Cheryl A. Kerfeld,§ Torbjörn Pascher,‡ and Villy Sundström‡

Department of Chemical Physics, Lund University, Box 124, S-221 00 Lund, Sweden, and Molecular Biology Institute, University of California, Los Angeles, California 90095

Received December 2, 2004; Revised Manuscript Received January 14, 2005

ABSTRACT: The cyanobacterial water-soluble orange carotenoid binding protein (OCP) is an ideal system for study of the effects of protein environment on photophysical properties of carotenoids. It contains a single pigment, the carotenoid 3′-hydoxyechinenone (hECN). In this study, we focus on spectroscopic properties of hECN in solution and in the OCP, aiming to elucidate the spectroscopic effects of the carotenoid−protein interaction in the context of the function(s) of the OCP. The noncovalent binding of hECN to the OCP causes a conformational change in the hECN, leading to a prolongation of the effective conjugation length. This change is responsible for shortening of the S_1 lifetime from 6.5 ps in solution to 3.3 ps in the OCP. The conformational change and the hydrogen bonding via the carbonyl group of hECN result in stabilization of an intramolecular charge-transfer (ICT) state. No signs of the ICT state were found in hECN in solution, regardless of the solvent polarity; spectral bands in transient absorption spectra of OCP-bound hECN exhibit features typical for the ICT state. Application of global fitting analysis revealed further effects of binding hECN in the OCP. The S_1 state of hECN in the OCP decays with two time constants of 0.9 and 3.3 ps. Modeling of the excited-state processes suggests that these two components are due to two populations of hECN in the OCP that differ in the hydrogen bonding via the carbonyl group. These results support the hypothesis that the OCP functions as a photoprotective shield under excess light. Mechanistically, the broadening of the hECN absorption spectrum upon binding to OCP enhances filtering effect of hECN. Furthermore, the binding-induced conformational change and activation of the ICT state that leads to a shortening of hECN lifetime effectively makes the protein-bound hECN a more effective energy dissipator.

Carotenoids are abundant natural pigments carrying out multiple functions in various biological systems (*1*−*4*). The broad functionality of carotenoids is directly related to the specific structure of their excited states. The strong absorption of carotenoids in the 350−550 nm region is due to a transition from the ground state (S_0), to the second excited state (S_2). Due to symmetry reasons, the lowest excited state (S_1) is not directly accessible from the ground state because the S_0−S_1 transition is symmetry forbidden (*1*). However, after being promoted to the S_2 state, an excited carotenoid molecule relaxes on the subpicosecond time scale to the S_1 state (*1*, *5*). Thus, knowledge of the spectroscopic properties of the S_1 state is crucial for a complete understanding of the light-driven functions of carotenoids in Nature.

A number of experimental and theoretical studies have been carried out in recent years to elucidate the properties of the S_1 state. The majority of these studies are focused on spectroscopic properties of carotenoids in solution, directed at better understanding the complexity of the excited-state manifold of carotenoids (see ref 1 for review). In proteins, most experimental and theoretical efforts are focused on understanding the roles of the S_1 state in the process of photosynthetic light harvesting, in which both S_2 and S_1 states are recognized as potential donors in carotenoid−(bacterio)-chlorophyll energy transfer (see ref 1 for review). In addition, a direct involvement of the carotenoid S_1 state in photoprotection in higher plants has been proposed (*6*−*9*), but this hypothesis still awaits verification (*10*).

One of the important, yet not fully understood, features of the carotenoid excited states is their response to a change of environment. In solution, several studies have shown that change of solvent properties usually has only a minor effect on the S_1 state, while the S_2 state is more sensitive (*1*, *5*). More recently, however, dramatic changes in the spectroscopic features of both the S_1 and S_2 states induced by a change of solvent have been revealed for a family of carotenoids that contain a conjugated carbonyl group in their structure (*11*−*13*). For these carotenoids, both energetics and dynamics of the excited states are significantly altered by a change in solvent polarity, and these effects are currently understood as being due to the presence of an intramolecular charge transfer (ICT) state that is stabilized in polar solvents (*11*−*14*). Moreover, the effects of polarity, hydrogen bonding, and the structure of carbonyl carotenoids are somehow

† The work at Lund University was supported by grants from the Swedish Research Council, the Wallenberg Foundation, and the Crafoord Foundation. T.Po. thanks the Swedish Energy Agency for financial support. C.A.K. acknowledges the support of the US Department of Agriculture (USDA 1999-01759).

* Corresponding author. E-mail: tomas.polivka@chemphys.lu.se. Phone: +46-46-222 4700. Fax: +46-46-2224119.

‡ Lund University.

§ University of California, Los Angeles.

10.1021/bi047473t CCC: $30.25
Published on Web 02/18/2005

synergistic, creating a complex picture of the excited-state properties containing some contradictory details (*15*−*18*).

In proteins, the effects of carotenoid−protein interactions on carotenoid excited states are even more elusive, and only a protein-induced shift of the S_2 state energy is a reliable measure of the carotenoid-protein interaction. Protein-induced effects on other important parameters, such as the lifetimes of the S_1 and S_2 states and the S_1 state energy, are not yet understood. This is mainly due to the limitations of the model systems used to date. Only carotenoids in light-harvesting proteins have so far been a subject of systematic study by means of advanced spectroscopic methods. In these proteins, changes in the abovementioned parameters caused by carotenoid−protein interactions are usually hidden, because the dynamical properties are inevitably determined by the carotenoid−(bacterio)chlorophyll energy transfer (*1*, *19*−*21*). On the other hand, knowledge of these parameters is required for reliable calculations of energy transfer efficiencies. For non-carbonyl carotenoids these effects are likely to be minor, thus the carotenoid excited-state properties can be, in the first approximation, replaced by those obtained from measurements in solution (*22*). In contrast, effects of the carotenoid−protein interaction are especially crucial for carbonyl carotenoids; these are the major light harvesting pigments in certain species of marine algae (*23*). It is proposed that it is the carotenoid−protein interaction that allows these carotenoids to transfer energy with high efficiency (*24*, *25*).

To discern the details of carotenoid−protein interactions, it is desirable to study the excited state properties in proteins that contain only a single carotenoid. To date, only a carotenoid-binding protein from the human retina has been investigated by time-resolved spectroscopic methods (*26*); although the results revealed the influence of binding on the excited state properties, lack of structural knowledge prevented assignment of the observed effects to specific amino acids. On the other hand, two crystal structures of carotenoproteins have been recently determined: the astaxanthin-binding protein, β-crustacyanin, responsible for the color of lobster shells was determined at 3.2 Å resolution (*27*) and the high-resolution (2.1 Å) structure of the orange carotenoid protein (OCP) from the cyanobacterium *Arthrospira maxima* (*28*). Here, we focus on study of the excited-state properties of the carotenoid in the *A. maxima* OCP.

The water-soluble OCP was first identified in 1981 (*29*). The crystal structure revealed that the protein is a homodimer, as expected from solution studies. Each 35 kDa subunit contains a single molecule of the carotenoid 3′-hydroxyechinenone (hECN).[1] hECN has a conjugated carbonyl group located at the terminus of a conjugated chain consisting of 11 C═C bonds (Figure 1). The crystal structure revealed several key features of carotenoid−protein interaction in the OCP. First, hydrogen bonds between the conjugated carbonyl group of the hECN molecule and Tyr203 and Trp290 residues were observed in the structure (Figure 1). The hydrogen-bonding amino acids are conserved in all known

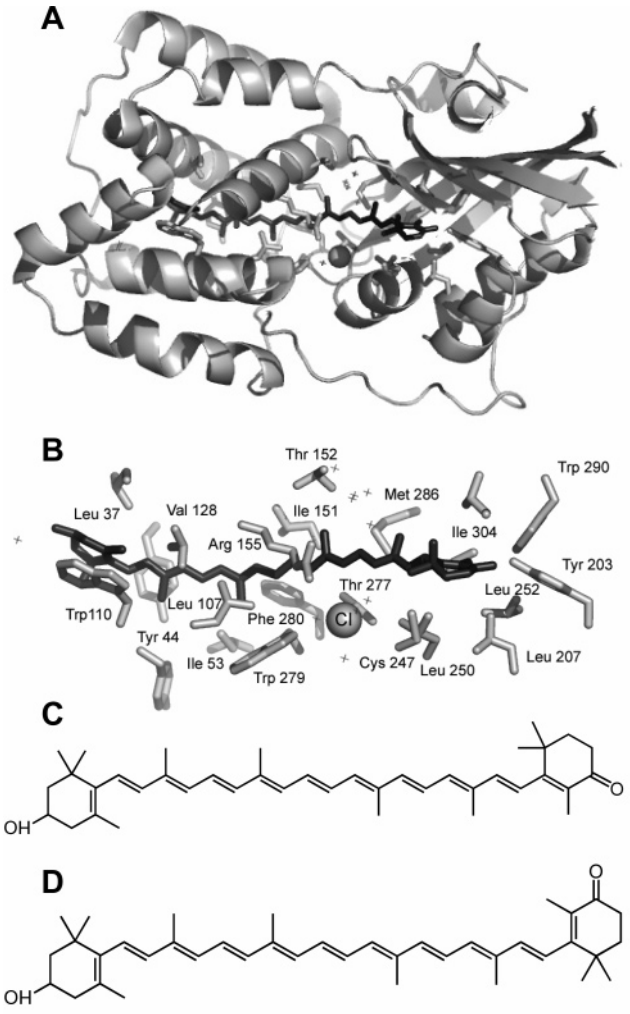

FIGURE 1: View of the (A) OCP and the (B) amino acid side chains (light gray) within 3.7 Å of the hECN molecule (dark gray). Water molecules are shown as crosses. A chloride ion, hydrogen bonded to the conserved residue Thr 277, is shown as a sphere. Chemical structure of hECN showing the orientation of the terminal ring containing the carbonyl group in (C) OCP and (D) solution. Panels A and B prepared with PYMOL (DeLano, W.L. (2002) The PyMOL Molecular Graphics System, www.pymol.org).

OCPs (*30*), suggesting they are functionally important. Furthermore, although the hECN molecule adopts an *all-trans* configuration in the OCP, it is bowed, exhibiting an average deviation of 16° from all-trans conformation (*28*). Another interesting feature of the OCP structure is that the binding pocket for the hECN is surrounded by an unusual number of methionine residues; this results in the positioning of six sulfur atoms within 6.5 Å of the hECN molecule.

Although the exact function of the OCP remains unknown, increasing transcript levels for the protein during exposure to intense light suggests possible involvement in photoprotection (*31*, *32*). The levels of the OCP transcript are also known to increase under salt stress (*33*), suggesting that expression of the protein may be evoked as part of a general stress response. Various hypotheses for the function of the OCP have been suggested (*30*), ranging from a carotenoid transport protein (*29*) to involvement in singlet oxygen quenching (*28*). The OCP can be also converted to another form, the red carotenoid protein (RCP), which is characterized by a red-shifted absorption spectrum (*30*). The OCP to

[1] Abbreviations: EADS, evolution associated difference spectra; EDTA, ethylenediaminetetraacetic acid; ESA, excited-state absorption; fwhm, full width half-maximum; hECN, 3′-hydroxyechinenone; ICT, intramolecular charge transfer; OCP, orange carotenoid protein; RCP, red carotenoid protein; SADS, species associated difference spectra.

RCP conversion is achieved either by proteolysis or by acidification of the OCP. It may be that hECN molecule in the RCP is more exposed to solvent (*30*), causing further red shift of hECN absorption spectrum. The RCP co-purifies with the OCP (*34*) and its function is not known, but it has a higher rate of singlet oxygen quenching (*28*), most likely due to increased solvent accessibility.

Here we report the characterization of the excited state dynamics of hECN both in solution and bound to the OCP in order to disclose the effects of hECN−protein interaction on excited states properties of the hECN. We develop several models to explain our observations in light of recent interpretations from other model systems. It is shown that incorporation of hECN into the OCP significantly alters both the energetics and the dynamics of the hECN excited states, and that these changes can be correlated with the protein−carotenoid interactions observed in the OCP structure.

MATERIALS AND METHODS

Sample Preparation. The OCP was isolated from the cyanobacterium *Arthrospira maxima* as described previously (*28*), dialyzed into 5 mM Tris pH 8, 0.5 M EDTA, 80 mM NaCl, and stored in the dark at −50 °C. Prior to the experiments, the OCP was diluted to an optical density of ∼0.1/mm at 495 nm. The sample was placed in a 2-mm quartz rotational cuvette (1.5 mL volume) and degassed by nitrogen. The carotenoid, hECN, was extracted by incubating a crude preparation of the OCP in ice-cold acetone for 15 min. The precipitated protein was separated by centrifugation (8 min, 10 000 rpm), resulting in a yellow-colored acetone extract of hECN. To remove any remaining protein, the extraction procedure was repeated five times, and the final extract was dried under vacuum. Since hECN is the only carotenoid in the OCP, and the absorption spectrum of the extracted hECN matches that published earlier (*35*), the extracted hECN was used without further purification. The dried hECN was stored in dark at −20 °C and dissolved prior to the experiments in *n*-hexane, methanol, or CS_2 purchased from Sigma Aldrich and used as received.

Spectroscopic Measurements. Steady-state absorption measurements were performed in a Jasco V-530 spectrophotometer in a 2 mm path length quartz cuvette. For the time-resolved measurements, femtosecond pulses were obtained from a Ti:Sapphire oscillator pumped by the 5 W output of a CW frequency-doubled, diode-pumped Nd:YVO_4 laser. The oscillator, operating at a repetition rate of 82 MHz, was amplified by a regenerative Ti:Sapphire amplifier pumped by a Nd:YLF laser (1 kHz), producing ∼130 fs pulses with an average energy of ∼0.9 mJ/pulse and a central wavelength at 800 nm. The amplified pulses were divided into two paths: one to pump an optical parametric amplifier for generation of excitation pulses, and the other to produce white-light continuum probe pulses in a 0.5 cm sapphire plate. The instrument response function was measured by frequency mixing the pump and probe pulses in a nonlinear crystal; the obtained cross-correlation was fitted to a Gaussian function with a fwhm of 120−150 fs, depending slightly on the wavelength of probing pulses. The mutual polarization of the pump and probe beams was set to the magic angle (54.7°) using a polarization rotator placed in the pump beam. For signal detection, the probe beam and an identical reference beam (that had no overlap with the pump beam) were focused onto the entrance slit of a spectrograph, which than dispersed both beams onto a home-built dual photodiode array detection system. Each array contained 512 photodiodes and allowed a spectral range of ∼270 nm to be measured in each laser shot. The spectral resolution of the detection system was ∼80 cm^{-1}, and the energy of excitation was attenuated by neutral density filters to ∼150 nJ/pulse giving an excitation density of $\sim 10^{15}$ photons $pulse^{-1}$ cm^{-2}. No sample degradation was observed during the course of measurement. Furthermore, absorption spectra were measured before and after measurements to ensure that no permanent photochemical changes occurred during the experiment.

Global Fitting. The transient absorption traces collected with the 512-element diode array were fitted globally to a sum of exponentials (*36*, *37*), including numerical deconvolution of the fwhm of the response function, and a fourth-degree polynomial describing the chirp. The fitting procedure used general linear regression for the amplitudes of the exponentials and the Nelder-Mead simplex method (*38*) for the rate constants, the fwhm and the chirp polynomial. To visualize time dynamics of the system, in the first approximation we assumed a sequential scheme with increasing lifetimes, and the resulting time constants were used to calculate spectral profiles of excited-state species in the sequential model. Following the terminology used in the recent review on global analysis, we call these spectra evolution-associated difference spectra (EADS) (*36*). Because in complicated systems EADS do not necessarily correspond to difference absorption spectra of particular excited states (*36*), we have applied target analysis to test different models for the excited-state dynamics. For the target analysis, the data was chirp-corrected before the fitting procedure using the chirp polynomial obtained from the global fitting. The rate constants of the target analysis were fitted using the Nelder-Mead simplex method. General linear regression was used to obtain difference spectra of the individual excited states in the target analysis. Again, in accordance with the terminology used by van Stokkum et al. (*36*), the difference spectra of the time components resulting from target analysis are called species-associated difference spectra (SADS).

RESULTS

Steady-State Absorption. Absorption spectra of hECN in three different solvents and in the OCP are compared in Figure 2. The absorption spectrum of hECN in the nonpolar solvent *n*-hexane exhibits a typical carotenoid-like shape, reflecting the strongly allowed S_0-S_2 transition with three distinct vibrational bands. The 0−0 vibrational peak is located at 476 nm. The moderate resolution of the vibrational bands is consistent with absorption spectra of other carotenoids in which the conjugation extends to various types of terminal rings (*39*). When hECN is dissolved in the polar solvent methanol, the spectral position of the 0−0 band remains the same, but the resolution of vibrational bands is further decreased, and the absorption spectrum is asymmetrically broadened toward the red. This polarity-induced behavior is characteristic of carotenoids possessing a conjugated carbonyl group in their structure, and it is a sign of an ICT state in the excited-state manifold (*12*, *13*). The interaction of hECN with the protein environment in the OCP

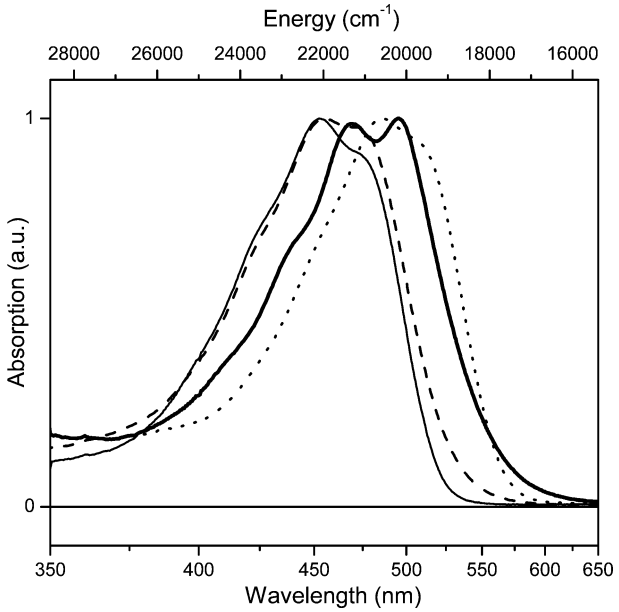

FIGURE 2: Absorption spectra of hECN in *n*-hexane (thin solid), methanol (dashed), and CS_2 (dotted). The absorption spectrum of the OCP is also shown (thick solid). All absorption spectra are normalized.

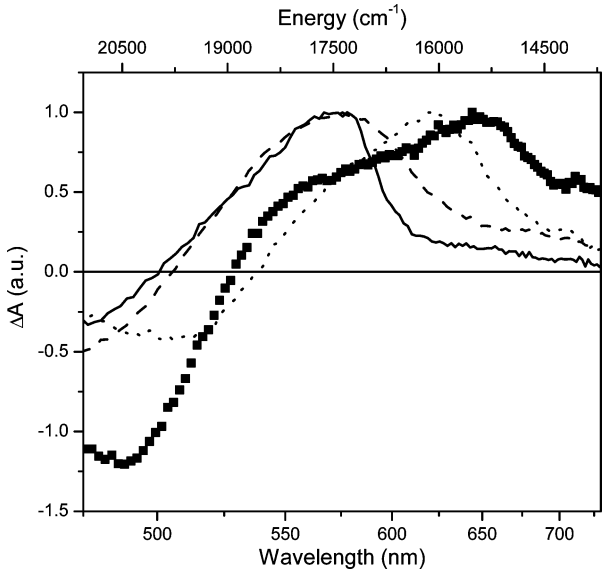

FIGURE 3: Transient absorption spectra of hECN in *n*-hexane (solid), methanol (dashed) CS_2 (dotted) and OCP (symbols). The transient spectra are recorded 1 ps after excitation at 485 nm (*n*-hexane and methanol), 495 nm (OCP) and 520 nm (CS_2). All spectra are normalized to the maximum of the ESA bands.

results in a red shift of the absorption spectrum; the lowest vibrational peak of hECN is located at 496 nm. This corresponds to a protein-induced shift of ~900 cm^{-1}, which is comparable to the shift observed for carotenoids in light-harvesting proteins (*20*, *40*). This suggests that the highly polarizable sulfur atoms of the methionine residues in close proximity to hECN in the OCP have probably little or no influence on the spectral shift. This interpretation is further substantiated by the absorption spectrum of hECN in CS_2 in which the 0−0 band appears at 512 nm; the polarizability-induced shift in CS_2 is significantly larger than that induced by association with the OCP.

Interestingly, however, the absorption spectrum of hECN in the OCP has well-resolved vibrational bands. In the OCP, the improvement in resolution of vibrational peaks is markedly larger than in other carotenoid-containing proteins. This effect could be attributed to a locked conformation of hECN in the OCP. In contrast, hECN in solution is expected to have a certain degree of conformational disorder. Inspection of the high-resolution structure reveals a possible reason for the well-resolved vibrational structure of hECN in the OCP. While in solution the C═C bond at both terminal rings takes the *s*-cis conformation in respect to the conjugated backbone (*39*, *41*), the OCP forces hECN to have this bond in *s*-trans position for the terminal ring containing the conjugated carbonyl group (*28*). As a result, the conjugated chain of hECN in the OCP is more linear than in solution (Figure 1), resulting in the observed highly resolved vibrational bands in the absorption spectrum (*1*, *39*).

Transient Absorption Spectra. The influence of the different environment on the spectroscopic properties of hECN is further emphasized in transient absorption spectra (Figure 3). The transient absorption spectra in the visible spectral region consist of ground-state bleaching and excited-state absorption (ESA) that corresponds to the well-known S_1-S_N transient of carotenoids (*1*). In solution, the polarity-induced behavior observed in steady-state absorption is further confirmed by transient absorption. In the nonpolar solvent *n*-hexane the S_1-S_N band peaks at ~575 nm. Almost the same maximum is observed also in the polar solvent methanol, but the S_1-S_N profile is broader than in *n*-hexane. No additional features are observed in the highly polarizable solvent CS_2, except the S_1-S_N transition peaks at 620 nm, reflecting a polarizability-induced shift of the S_N state, because the S_1 state energy is not (or very little) affected by solvent polarizability (*1*).

As in the steady-state absorption spectra, the most pronounced changes are exhibited when hECN is embedded in the OCP. The ESA band is extremely red shifted, having its maximum at 650 nm. The large red shift of the ESA band is prominent in comparison to the S_1-S_N profile in CS_2 (dotted line in Figure 3). The red shift of the absorption spectrum of hECN in CS_2 is larger than that in the OCP (Figure 2). In contrast, for the S_1-S_N ESA the effect is the opposite; the OCP ESA peak is shifted 30 nm to the red as compared to that measured for hECN in CS_2. Moreover, the OCP ESA is much broader than the S_1-S_N band of hECN in solution. In fact, the ESA band of hECN in the OCP apparently consists of two bands, the weaker one being visible as a pronounced shoulder at 565 nm. The main 650 nm band is due to stabilization of the ICT state in the OCP (see Discussion).

Kinetics. To characterize dynamical properties of the excited states of hECN in various environments, all 512 kinetic traces recorded in the 470−750 nm region were analyzed globally (*36*). The fitting results and the kinetics measured at selected wavelengths in *n*-hexane and in the OCP are shown in Figure 4. In *n*-hexane, the fitting procedure results in two time constants of 0.23 and 6.3 ps. The origin of these two components can be deduced from the evolution-associated difference spectra (EADS, see Experimental section) shown in Figure 5. The first EADS (thin line) created by excitation consists of a ground-state bleaching and stimulated emission from the S_2 state, manifested as two negative bands located at 470 and 520 nm. The ESA signal

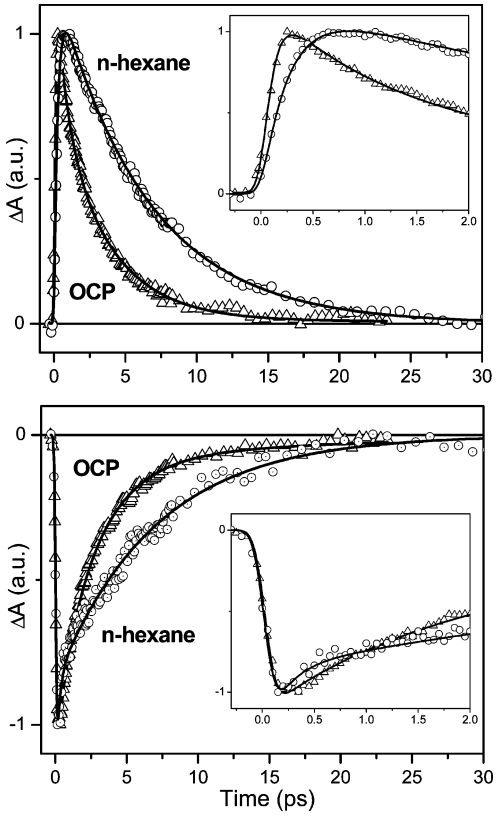

FIGURE 4: Kinetics measured at the maximum of the ESA (top) and bleaching (bottom) bands of hECN in *n*-hexane and in the OCP. For kinetics measurements in *n*-hexane, excitation was at 485 nm and probing at 575 nm (top) and 475 nm (bottom); in OCP the excitation was at 495 nm and probing wavelengths were 650 nm (top) and 490 nm (bottom). The insets show dynamics in the first two picoseconds after excitation.

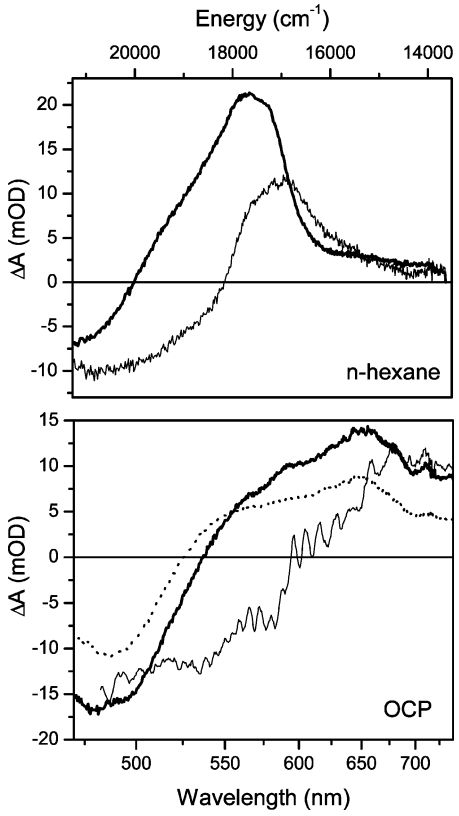

FIGURE 5: EADS resulting from the global fitting analysis of the following: (top) hECN in *n*-hexane, EADS corresponding to the species with 0.23 ps (thin line) and 6.4 ps (thick line) lifetimes; (bottom) hECN in the OCP. The lifetimes of species associated with the EADS are <0.1 ps (thin line), 0.9 ps (thick line), and 3.3 ps (dotted line).

above 550 nm indicates that this EADS does not represent a pure S_2 spectrum; most likely it is contaminated by a contribution from a hot S_1 state. However, adding a fast component to the fitting scheme does not allow for separation of the S_2 and hot S_1 contributions, because the S_2 stimulated emission still remains at delays longer than 200 fs. This suggests that S_2-S_1 internal conversion and S_1 vibrational relaxation take place on a comparable time scale. Within 230 fs the first EADS is replaced by the second one (thick line), which exhibits a typical S_1-S_N profile. The second EADS decays in 6.3 ps to form the hECN ground state. Consequently, while the 6.3 ps component is clearly due the S_1 lifetime, the 230 fs component should be taken as an upper limit for the S_2 lifetime, because of the abovementioned mixing with the S_1 vibrational relaxation. It is worth noting that global fits can be slightly improved by adding a third decay component that may be due to some equilibration process in the S_1 state (data not shown, see footnote to Table 1). However, because the amplitude of the additional component is less than 5%, we omit this component in our analysis. A similar decay pattern was observed also in methanol and CS_2 (Table 1), suggesting that the excited-state dynamics of hECN are not (or very little) affected by the solvent parameters. However, when hECN is bound to OCP, the global fitting gives a different decay pattern than that obtained for hECN in solution. First, as shown in Figure 4, both the S_2 and S_1 lifetimes are significantly shorter in the OCP, ~90 fs and 3.3 ps, respectively. Moreover, in

Table 1: Time Constants Obtained from the Global Fitting Analysis[a]

solvent	τ_1 (ps)	τ_2 (ps)	τ_3 (ps)[b]
CS_2	0.135	6.8	–
n-hexane	0.230	6.4	–
methanol	0.185	6.2	–
OCP	<0.1	3.3	0.9

[a] The standard error of the time constants is in the range 5−10%. [b] For *n*-hexane and CS_2, an additional low-amplitude decay component with a time constant of 1.2 ± 0.5 ps (CS_2) and 2.1 ± 0.7 ps (*n*-hexane) slightly improves the global fit. The amplitude of this component does not exceed 5% in *n*-hexane and 10% in CS_2.

contrast to hECN in solution, these two components are not sufficient for obtaining satisfying fits, and an additional component with 0.9 ps time constant is needed. The EADS (Figure 5b) gives more information about the origin of the decay components. The EADS formed by the excitation pulse (thin line) is similar to that obtained from global fitting of the data taken on hECN in solution. This EADS decays in ~90 fs to form another one depicted as a thick line, which then decays within 0.9 ps to create the final EADS (dotted line, Figure 5b), which decays in 3.3 ps to form the ground-state hECN. It is apparent that the 0.9 ps component is most pronounced in the main ESA band at 650 nm. Due to the dominance of the 0.9 ps component in the red part of the ESA band, it is tempting to assign it to vibrational relaxation in the S_1 state or to the ICT stabilization because these processes are known to occur on a similar time scale (*16*, *42*, *43*). However, the presence of this component in kinetics

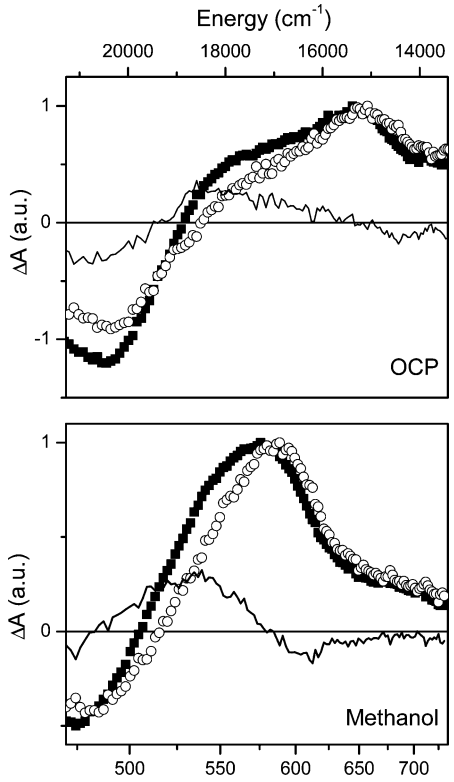

FIGURE 6: Transient absorption spectra of hECN in the OCP (top) excited at 495 nm (full symbols) and 530 nm (open symbols). The bottom panel shows the corresponding transient absorption specra of hECN in methanol excited at 485 nm (full symbols) and 520 nm (open symbols). All spectra are normalized to the maximum of the ESA band. The lines show the difference between blue and red excitation.

of ground state recovery below 500 nm (Figure 5) does not support this assignment. Instead, the presence of the 0.9 ps component in the bleaching region shows that a part of the excited state population decays directly to the ground state with the 0.9 ps time constant (see Discussion).

Excitation Wavelength Dependence. Recent experiments on carotenoid excited-state properties showed that excitation into higher or lower energy tails of the absorption spectrum can result in different excited-state dynamics (*16*, *18*, *44*). Since the excitation wavelength dependence observed earlier for another carbonyl carotenoid, peridinin, was related to hydrogen bonding via conjugated carbonyl group (*16*), we have carried out experiments using excitation in various parts of absorption spectrum (Figure 6). Both in the OCP and in methanol, moving the excitation of the OCP into the red tail of the absorption spectrum does not shift the S_1-S_N band. However, the intensity of the signal is reduced in the high-energy part of the S_1-S_N band, in accord with observations for peridinin in protic solvents (*16*, *18*). In the OCP, the excitation at different wavelengths changes spectral profiles of the excited state species having the 3.3 and 0.9 ps lifetimes, as demonstrated by the EADS (Figure 7). The excitation wavelength dependence confirms that the 0.9 ps component is more pronounced within the 650-nm band, while dynamics of the 565-nm shoulder is dominated by the 3.3-ps component. After 530-nm excitation the 565-nm shoulder is nearly missing. Together, these results point to a unique decay pattern of hECN excited states when the pigment is associated with the OCP.

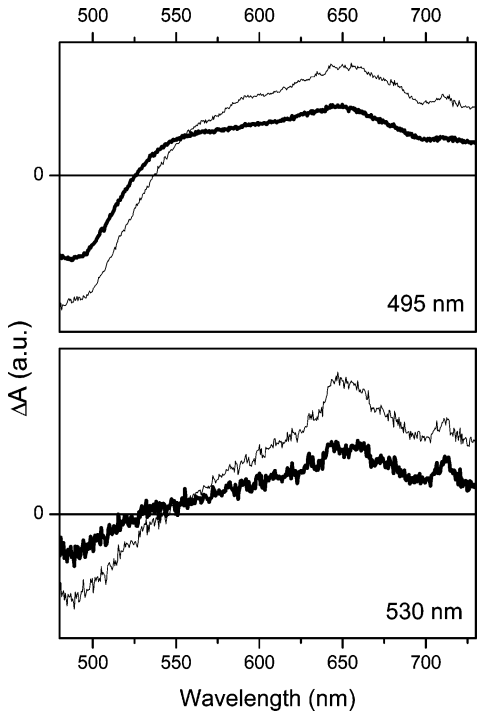

FIGURE 7: EADS resulting from the global fitting of kinetics of hECN in the OCP excited at 495 nm (top) and 530 nm (bottom). The spectra represents spectral profiles of excited-state species associated with the 0.9 ps (thin line) and 3.3 ps (thick line) components.

DISCUSSION

hECN in Solution. Our observations of the solvent-dependent behavior of hECN are in accord with the current understanding of the relation between the structure of carbonyl carotenoids and the magnitude of polarity-induced changes. Since the conjugated C═C backbone of hECN is relatively long, nine C═C bonds in the linear arrangement and two additional C═C bonds in the *s-cis* orientation located in the terminal β-rings (Figure 1), the C═O group located in one of the terminal rings is well separated from the main conjugated backbone. As demonstrated by studies of different carbonyl carotenoids, this conformation would be predicted to be only mildly affected by solvent polarity (*12*, *13*). We observed that the only pronounced effect of solvent polarity on the spectroscopic properties of hECN is the change in the absorption spectrum upon going from *n*-hexane to methanol (Figure 1). The slight loss of vibrational structure and the asymmetric broadening toward red in methanol are similar to the polarity-induced effects observed for other carbonyl carotenoids. Likewise, a weak effect is observed for the S_1-S_N transition; the small increase of signal at the red part of the S_1-S_N band in methanol is possibly attributable to the presence of the ICT state (Figure 3). The S_1 lifetime, which in carbonyl carotenoids is usually dramatically changed by the solvent polarity (*12*, *13*), remains, within the experimental error, the same in all solvents used here, ~6.5 ps. In summary, hECN exhibits the weakest polarity-induced effects observed so far among the carbonyl carotenoids. Its behavior is most similar to the carotenoid spheroidenone, which has a linear 10 C═C chain with the carbonyl group attached at the end in an *s*-cis orientation (*13*). In hECN, extension of the conjugation to the carbonyl group and the terminal rings further diminishes the polarity-

induced behavior, underscoring the importance of the position of the carbonyl group with respect to the conjugated backbone in influencing the magnitude of polarity effects.

hECN in OCP. The hECN binding cleft in the OCP is lined by a number of nonpolar amino acids with the carbonyl group nestling into a pocket formed by polar residues (Figure 1) (*28*). The protein environment, the hydrogen bonding via the carbonyl group, and the conformational change of hECN induced by interaction with the protein underline unusual spectroscopic properties of the OCP. Therefore, one of the key questions is whether the protein provides an environment that stabilizes the ICT state in hECN. Although the well-resolved vibrational bands in the absorption spectrum of a carbonyl carotenoid are usually characteristic of an ICT-silent lowest excited state (*12*, *13*), in the OCP the asymmetric broadening of the absorption spectrum and the spectral features observed in the transient absorption spectra suggest that the ICT state is stabilized. The loss of vibrational structure of carbonyl carotenoids in polar solvents was suggested to be due to increased conformational disorder (*12*, *13*, *16*). However, confinement of the hECN in the OCP prevents formation of conformers, thereby preserving the well-resolved vibrational structure even though the carbonyl group experiences a polar environment. On the other hand, the asymmetric broadening of the absorption spectrum can be attributed to the hydrogen bonding via the carbonyl group observed in the OCP (*28*). The relation between asymmetric broadening and hydrogen bonding is further substantiated by the absorption spectrum of another OCP, isolated from *Anacystis nidulans*. This protein binds zeaxanthin, which lacks the conjugated carbonyl group, and the absorption spectrum shows no signs of the asymmetric broadening (*45*).

S_1 Lifetime. The presence of the ICT state in the OCP may imply that, as in the majority of carbonyl carotenoids, the shortening of the S_1 lifetime in the OCP is related to the stabilization of the ICT state (*12*, *13*). However, it is also necessary to keep in mind that the conformational change of hECN in the OCP (Figure 1) leads to a longer effective conjugation and, consequently, shorter S_1 lifetime (*1*). In solution, hECN adopts a conformation in which 9 conjugated C═C bonds form the linear backbone and 2 C═C bonds are in *s-cis* orientation in respect to this backbone (Figure 1). In terms of effective conjugation length (N_{eff}), a conjugated C═C group in *s*-cis orientation contributes by ~0.5 (*39*), and a similar value can be taken for extension of conjugation to the C═O group (*1*). Consequently, in solution the effective conjugation length is $N_{eff} = 9 + 2 \times 0.5 + 0.5 = 10.5$. The "linearization" of hECN in the OCP converts one of the C═C bonds located at the terminal ring to *s*-trans orientation, and N_{eff} is changed to $N_{eff} = 10 + 0.5 + 0.5 = 11$. Comparing the S_1 lifetime of hECN in solution and in the OCP with the S_1 lifetimes of the carotenoids spheroidenone ($N_{eff} = 10.5$) and lycopene ($N_{eff} = 11$), which are 6 and 4 ps, respectively (*1*), suggests that the conformational change represents a major contribution to the shortening of the S_1 lifetime of hECN in the OCP. In fact, the difference between the measured value of 3.3 ps and the value of ~4 ps expected for a carotenoid with $N_{eff} = 11$ may be related to the fact that the C═O group of hECN in the OCP is in *s*-trans position with respect to the rest of the conjugated system. In this orientation, it is likely that it contributes slightly more than 0.5 to N_{eff}, further shortening the S_1 lifetime. Thus, we conclude that the shorter lifetime of hECN in the OCP relative to that in solution is caused by the conformational change of hECN in the OCP binding pocket. Similar shortening of the S_1 lifetime due to the linearization of the conjugated chain has been also observed for astaxanthin in α-crustacyanin (*46*).

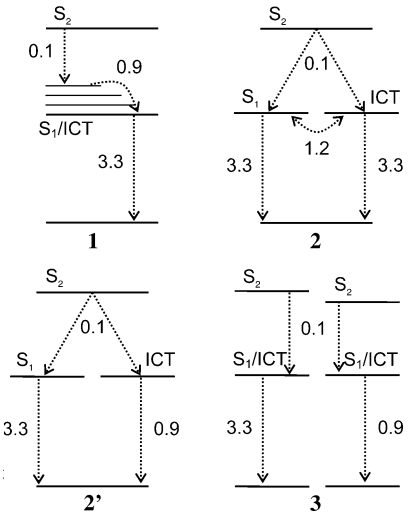

FIGURE 8: Schematic models of the excited-state dynamics of hECN in the OCP. See text for details.

Origin of the Spectral Bands in the Transient Absorption Spectra. Transient absorption spectra further support the hypothesis of an active ICT state in the OCP. Since the conjugated chain of hECN is linear in the OCP, in the ICT-silent case one would expect a narrow, structureless S_1-S_N band (*1*). On the contrary, the observed transient absorption spectra of the OCP exhibit an extremely broad ESA consisting of two spectral features located at 565 and 650 nm. Except for the spectral position of the ESA bands, the transient absorption spectrum of the OCP closely resembles those previously observed for the carbonyl carotenoid peridinin in various polar solvents. The peridinin spectra were interpreted in terms of the $ICT-S_N$ (main band) and S_1-S_N (blue shoulder) transitions (*12*, *13*, *16*, *18*). Accordingly, in the OCP, we assign the 650 nm ESA band as a result of the $ICT-S_N$ transition, while the blue shoulder originates from the S_1-S_N transition.

Relaxation Pathways. Having established that the shortening of the S_1 lifetime is not related to polarity but is caused by the conformational change of hECN in the OCP, the key question is what is the origin of the 0.9 ps decay component specific to hECN when enclosed by the OCP. To answer this, we have applied different relaxation schemes (Figure 8), and we will discuss how well these models concur with the results of global fitting.

In Model 1, the 0.9 ps component is assigned to a relaxation within the S_1/ICT state, which is in accord with previous findings for peridinin (*16*−*18*). However, for hECN in the OCP, the 0.9 ps component also appears as decay in the bleaching region, precluding such an assignment. If the 0.9 ps component were connected with an excited-state process, the bleaching recovery should be free from this component, unless there is a substantial ESA in the 460−500 region rising with the 0.9 ps component. Since such a band has never been observed for carotenoids, we conclude that the presence of the 0.9 ps component in the bleaching

region indicates that a part of the hECN excited-state population decays to the ground state with the 0.9 ps time constant. Consequently, we rule out the Model 1.

For our second model, we again consider the recent studies of peridinin in the protic polar solvent methanol. A global fitting of peridinin kinetics revealed two decay components, with their amplitudes varying with excitation wavelength (*16*, *18*), which, with the exception of the different values of the time constants, is the same situation as observed here for hECN in the OCP. Therefore, our second scheme is based on the model of excited-state dynamics of peridinin suggested by Papagiannakis et al. (*18*) in which the S_1 and ICT states are considered to be separate electronic excited states, and the 0.9 ps component is related to the equilibration between the S_1 and ICT populations. Since the 0.9 ps component represents a sum of the S_1 (or ICT) decay and S_1-ICT equilibration (Figure 8, scheme 2), it is expected to appear in the ground-state bleaching. The results could then be explained by an excitation wavelength-dependent branching ratio of the S_2 decay. In this model, the direction of population transfer between the S_1 and ICT states is determined from the sign of the time evolution of the signal (decay vs rise). Therefore, the pronounced decay of the 0.9 ps component within the 650 nm band predicts that the equilibration would preferentially move the population from the ICT state to the S_1 state. However, this is contrary to the current understanding of excited states of carbonyl carotenoids (based mostly on detailed experiments on peridinin) that the ICT state lies below the S_1 state (*12*, *13*, *18*, *47*). The fit of the OCP data to Model 2 can be partially improved by assuming that there is no communication between the S_1 and ICT states (denoted as Model 2′ in Figure 8), and that these two states have lifetimes of 3.3 and 0.9 ps, respectively. Then, the excitation into the red part of the absorption spectrum favors population of the ICT state, resulting in a loss of the S_1-S_N band with the 0.9 ps lifetime becoming the major component in the 650 nm band (Figure 7). Nevertheless, in this modified Model 2, the 3.3 ps component still has substantial amplitude in the ICT$-S_N$ region even if the S_1-S_N band is not present (Figure 7), challenging the assignment of the 3.3 ps lifetime to the S_1 state. Furthermore, the applied assumption of no communication between the S_1 and ICT states contradicts all current models of excited-state dynamics of carbonyl carotenoids (*15*−*18*). Thus, the Model 2′ also fails to explain the excited-state dynamics of hECN in the OCP.

A third possible interpretation is based on a model for peridinin proposed by Zigmantas et al. to explain the excitation wavelength dependence of peridinin dynamics in protic solvents (*16*). In this model, the S_1 and ICT states are strongly coupled, forming a common S_1/ICT state having a complicated potential surface, on which the S_1 and ICT states are represented as potential minima separated by a low energy barrier. In terms of Model 3, the 0.9 and 3.3 ps components are the S_1/ICT lifetimes of two different hECN populations. Both populations have similar transient absorption spectra, but they differ in the ratio between the S_1-like (565 nm band) and ICT-like (650 nm band) transitions. While the population excited predominantly at 490 nm has a substantial S_1-like contribution and a lifetime of 3.3 ps, the hECN molecules largely excited at 530 nm have a S_1/ICT lifetime of 0.9 ps and exhibit a less pronounced 565 nm band.

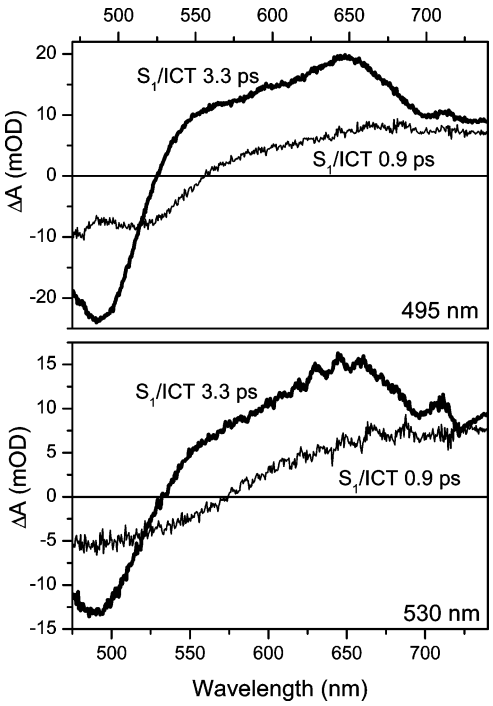

FIGURE 9: SADS of the S_1/ICT states resulting from target analysis according to the Model 3 in Figure 8. Excitation wavelengths were 495 nm (top) and 530 nm (bottom). See text for details.

In other words, the hECN molecules absorbing in the red region have the enhanced ICT character of the S_1/ICT state. This is in accordance with the hypothesis that hydrogen bonding via the carbonyl group intensifies the ICT character of the S_1/ICT state (*16*), because the red wing of the absorption spectrum is formed by hydrogen bonding. To apply this model to the OCP, we used target analysis to fit the data measured after 495 and 530 nm excitation according to the Model 3. The resulting SADS of the two S_1/ICT populations are shown in Figure 9. For both excitation wavelengths, the excited-state population decaying with the 3.3 ps component has a pronounced S_1-like shoulder, as expected for an S_1/ICT state having moderate ICT character. The fast decaying population exhibits a SADS dominated by a broad structureless band extending beyond 700 nm. The S_1-like signal is nearly missing, especially for the 530 nm excitation. Also, the fraction of the population decaying with the 0.9 ps time constant has a red-shifted bleaching, in agreement with the assumption that this excited-state population is created by excitation of hECN molecules absorbing in the red wing of the absorption spectrum. In this model, the 0.9 ps S_1/ICT lifetime of a fraction of the hECN population cannot be explained solely by linearization of the conjugated chain as described above, and, similarly to peridinin (*16*), hydrogen bonding underlies a short S_1/ICT lifetime.

Although this model obviously best fits the experimental data, it implies the presence of at least two populations of hECN in the OCP differing in hydrogen bonding via the carbonyl group. This result seems to conflict with the structural data (*28*), in which there are hydrogen bonds involving Trp 290 and Tyr203 (2.8 and 2.7 Å from the carbonyl oxygen of the hECN; Figure 1b). Both molecules in the asymmetric unit of the crystallized OCP were refined independently and both contain these hydrogen bonds. The structure was determined from X-ray diffraction data col-

lected on flash frozen crystals at 100 K. In contrast, at room temperature the hydrogen bonding is likely to be a dynamical process involving rapid breaking and re-formation of the bond. Consequently, there may exist an equilibrium between hECN molecules with and without hydrogen bond. Because there are two amino acid residues involved in the hydrogen bonding (*28*), the interaction between the carbonyl oxygen and the protein may vary for different OCPs in the sample, leading to the two hECN populations. However, it must be noted that Model 3 cannot fully account for the data; the SADS of the two S_1/ICT states are not identical after 495 and 530 nm excitations. The S_1/ICT state decaying with 0.9 ps has a weak S_1-like shoulder after 495 nm excitation, but this shoulder is absent after excitation at 530 nm (Figure 9). This suggests that the situation is more complicated than outlined in Figure 8, and a distribution of the hECN molecules with slightly different excited state properties probably better describes the OCP. Furthermore, it is worth noting that in order to fully explain the OCP excited state dynamics it may be necessary to take into account effects that were not considered here. For example, breaking of hydrogen bonds upon excitation. This effect has recently been observed in photoactive yellow protein (PYP) by mid-infrared femtosecond spectroscopy (*48*). In the PYP, the hydrogen bond between the carbonyl group of the chromophore and a cysteine residue is broken upon excitation. Since the time scale of this process is comparable to the 0.9 ps decay component observed here, such an effect cannot be ruled out for the OCP.

Functional Implications. The important question is how the effects described above are related to possible functions of the OCP. Although involvement of the OCP in photoprotection of cyanobacteria has been demonstrated by an increase of the OCP transcript levels under high-light and UV-light stress (*31*, *32*), the photoprotective mechanisms are still elusive. One suggested mechanism involves accumulation of the OCP at the outer membrane or cell wall of cyanobacteria, where the proteins are arranged to form a photoprotective shield (*30*, *49*). Even though this function could be in fact carried out by any carotenoid in the absence of protein, the binding of hECN to the OCP improves the carotenoid's photoprotective properties in several ways. First, hydrogen bonding via the carbonyl group broadens the absorption spectrum of the protein-bound hECN, enabling filtering across a broader spectral range relative to that of free hECN. Second, binding to the protein shortens the S_1 lifetime of hECN by changing the conformation of the carotenoid, making the dissipation of absorbed energy more efficient. It must be noted, however, that this effect likely plays only a minor role under the light intensities occurring in the natural habitats of cyanobacteria, suggesting that the shortening of the hECN lifetime is not the primary photoprotective mechanism. Nevertheless, our results show that binding to the OCP increases the ability of hECN to absorb and dissipate light energy and, consequently, supports the hypothesis of the OCP playing the role of a light filter in cyanobacteria under light stress.

REFERENCES

1. Polívka, T., and Sundström, V. (2004) Ultrafast dynamics of carotenoid excited states. From solution to natural and artificial systems, *Chem. Rev. 104*, 2021−2071.
2. Frank, H. A., and Cogdell, R. J. (1996) Carotenoids in photosynthesis, *Photochem. Photobiol. 63*, 257−264.
3. El Agamey, A., Lowe, G. M., McGarvey, D. J., Mortensen, A., Phillip, D. M., Truscott, T. G., and Young, A. J. (2004) Carotenoid radical chemistry and antioxidant/pro-oxidant properties, *Arch. Biochem. Biophys. 430*, 37−48.
4. Landrum, J. T., and Bone, R. (2001) Lutein, zeaxanthin, and the macular pigment, *Arch. Bioch. Biophys. 385*, 28−40.
5. Macpherson, A. N., and Gillbro, T. (1998) Solvent dependence of the ultrafast S_2-S_1 internal conversion rate of β-carotene, *J. Phys. Chem. A 102*, 5049−5058.
6. Frank, H. A., Cua, A., Chynwat, V., Young, A., Gosztola, D., and Wasielewski, M. R. (1994) Photophysics of the carotenoids associated with the xanthophyll cycle in photosynthesis, *Photosynth. Res. 41*, 389−395.
7. Bassi, R., and Caffari, S. (2000) Lhc proteins and the regulation of photosynthetic light harvesting function by xanthophylls, *Photosynth. Res. 64*, 243−256.
8. Polívka, T., Zigmantas, D., Sundström, V., Formaggio, E., Cinque, G., and Bassi, R. (2002) Carotenoid S_1 state in a recombinant light-harvesting complex of photosystem II, *Biochemistry 41*, 439−450.
9. Ma, Y.-Z., Holt, N. E., Li, X.-P., Niyogi, K., and Fleming, G. R. (2003) Evidence for direct carotenoid involvement in the regulation of photosynthetic light harvesting, *Proc. Natl. Acad. Sci. U.S.A. 100*, 4377−4382.
10. Holt, N. E., Fleming, G. R., and Niyogi, K. K. (2004) Toward an understanding of the mechanism of nonphotochemical quenching in green plants, *Biochemistry 43*, 8281−8289.
11. Bautista, J. A., Connors, R. E., Raju, B. B., Hiller, R. G., Sharples, F. P., Gosztola, D., Wasielewski, M. R., and Frank, H. A. (1999) Excited-state properties of peridinin: Observation of a solvent dependence of the lowest excited singlet state lifetime and spectral behavior unique among carotenoids, *J. Phys. Chem. B 103*, 8751−8758.
12. Frank, H. A., Bautista, J. A., Josue, J., Pendon, Z., Hiller, R. G., Sharples, F. P., Gosztola, D., and Wasielewski, M. R. (2000) Effect of the solvent environment on the spectroscopic properties and dynamics of the lowest excited states of carotenoids, *J. Phys. Chem. B 104*, 4569−4577.
13. Zigmantas, D., Hiller, R. G., Sharples, F. P., Frank, H. A., Sundström, V., and Polívka, T. (2004) Effect of a conjugated carbonyl group on the photophysical properties of carotenoids, *Phys. Chem. Chem. Phys. 6*, 3009−3016.
14. Vaswani, H. M., Hsu, C.-P., Head-Gordon, M., and Fleming, G. R. (2003) Quantum chemical evidence for an intramolecular charge-transfer state in the carotenoid peridinin of peridinin-chlorophyll-protein, *J. Phys. Chem. B 107*, 7940−7946.
15. Shima, S., Ilagan, R. P., Gillespie, N., Sommer, B. J., Hiller, R. G., Sharples. F. P., Frank, H. A., and Birge, R. R. (2003) Two-photon and fluorescence spectroscopy and the effect of environment on the photochemical properties of peridinin in solution and in the peridinin-chlorophyll-protein from *Amphidinium carterae*, *J. Phys. Chem. A 107*, 8052−8066.
16. Zigmantas, D., Hiller, R. G., Yartsev, A., Sundström, V., and Polívka, T. (2003) Dynamics of excited states of the carotenoid peridinin in polar solvents: Dependence on excitation wavelength, viscosity, and temperature, *J. Phys. Chem. B 107*, 5339−5348.
17. Linden, P. A., Zimmermann, J., Brixner, T., Holt, N. E., Vaswani, H. M., Hiller, R. G., and Fleming, G. R. (2004) Transient absorption study of peridinin and peridinin-chlorophyll a-protein after two-photon excitation, *J. Phys. Chem. B 108*, 10340−10345.
18. Papagiannakis, E., Larsen, D. S., van Stokkum, I. H. M., Vengris, M., Hiller, R. G., and van Grondelle, R. (2004) Resolving the excited state equilibrium of peridinin in solution, *Biochemistry 43*, 15303−15309.
19. Papagiannakis, E., Kennis, J. T. M., van Stokkum, I. H. M., Cogdell, R. J., and van Grondelle, R. (2002) An alternative carotenoid-to-bacteriochlorophyll energy transfer pathway in photosynthetic light harvesting, *Proc. Natl. Acad. Sci. U.S.A. 99*, 6017−6022.
20. van Amerongen, H., and van Grondelle, R. (2001) Understanding the energy transfer function of LHCII, the major light-harvesting complex of green plants, *J. Phys. Chem. B 105*, 604−617.
21. Zhang, J.-P., Fujii, R., Qian, P., Inaba, T., Mizoguchi, T., Koyama, Y., Onaka, K., Watanabe, Y., and Nagae, H. (2000) Mechanism of the carotenoid-to-bacteriochlorophyll energy transfer via the S_1 state in the LH2 complexes from purple bacteria, *J. Phys. Chem. B 104*, 3683−3691.

22. Polívka, T., Zigmantas, D., Herek, J. L., He, Z., Pascher, T., Pullerits, T., Cogdell, R. J., Frank, H. A., and Sundström, V. (2002) The carotenoid S_1 state in LH2 complexes from purple bacteria *Rhodobacter sphaeroides* and Rhodopseudomonas acidophila: S-1 energies, dynamics, and carotenoid radical formation, *J. Phys. Chem. B 106*, 11016−11025.
23. Hiller, R. G. (1999) Carotenoids as components of the light-harvesting proteins of eucaryotic algae, in *Photochemistry of Carotenoids* (Frank, H. A., Young, A. J., Britton, G., and Cogdell, R. J., Eds.) pp 81−98, Dordrecht, The Netherlands.
24. Zigmantas, D., Hiller, R. G., Sundström, V., and Polívka, T. (2002) Carotenoid to chlorophyll energy transfer in the peridinin-chlorophyll-a-protein complex involves an intramolecular charge transfer state, *Proc. Natl. Acad. Sci. U.S.A. 99*, 16760−16765.
25. Krueger, B. P., Lampoura, S. S., van Stokkum, I. H. M., Papagiannakis, E., Salverda, J. M., Gradinaru, C. C., Rutkauskas, D., Hiller, R. G, and van Grondelle, R. (2001) Energy transfer in the peridinin chlorophyll-a protein of Amphidinium carterae studied by polarized transient absorption and target analysis, *Biophys. J. 80*, 2843−2855.
26. Billsten, H. H., Bhosale, P., Yemelyanov, A., Bernstein, P. S., and Polívka, T. (2003) Photophysical properties of xanthophylls in carotenoproteins from human retina, *Photochem. Photobiol. 78*, 138−145.
27. Cianci, M., Rizkallah, P. J., Olczak, A., Raftery, J., Chayen, N. E., Zagalsky, P. F., and Helliwell, J. R. (2002) The molecular basis of the coloration mechanism in lobster shell: β-crustacyanin at 3.2 Å resolution, *Proc. Natl. Acad. Sci. U.S.A. 99*, 9795−9800.
28. Kerfeld, C. A., Sawaya, M. R., Brahmandam, V., Cascio, D., Ho, K. K., Trevithick-Sutton, C. C., Krogmann, D. W., and Yeates, T. O. (2003) The crystal structure of a cyanobacterial water-soluble carotenoid binding protein, *Structure 11*, 55−65.
29. Holt, T. K., and Krogmann, D. W. (1981) A carotenoid-protein from cyanobacteria, *Biochim. Biophys. Acta 637*, 408−414.
30. Kerfeld, C. A. (2004) Structure and function of the water-soluble carotenoid-binding proteins of cyanobacteria, *Photosynth. Res. 81*, 215−225.
31. Hihara, Y., Kamei, A., Kanehisa, M., Kaplan, A., and Ikeuchi, M. (2001) DNA microarray analysis of cyanobacterial gene expression during acclimation to high light, *Plant Cell 13*, 793−806.
32. Huang, L., McCluskey, M. P., Ni, H., and LaRossa, R. A. (2002) Global gene expression profiles of the cyanobacterium *Synechocystis* sp. strain PCC 6803 in response to irradiation with UV−B and white light, *J. Bacteriol. 184*, 6845−6858.
33. Kanesaki, Y., Suzuki, I., Allakhverdiev, S. I., Mikami, K., and Murata, N. (2002) Salt stress and hyperosmotic stress regulate the expression of different sets of genes in *Synechocystis* sp. PCC 6803, *Biochem. Biophys. Res. Comm. 290*, 339−348.
34. Wu, Y. P., and Krogmann, D. W. (1997) The orange carotenoid protein of *Synechocystis* PCC 6803, *Biochim. Biophys. Acta 1322*, 1−7.
35. Mercadante, A. Z., and Egeland, E. S. (2004) in *Carotenoids, Handbook* (Britton, G., Liaaen-Jensen, S., and Pfander, H., Eds.) Birkhäuser Verlag, Basel, Switzerland.
36. van Stokkum, I. H. M., Larsen, D. S., and van Grondelle, R. (2004) Global and target analysis of time-resolved spectra, *Biochim. Biophys. Acta 1657*, 82−104.
37. Beechem, J. M. (1992) Global analysis of biochemical and biophysical data, *Methods Enzymol. 210*, 37−54.
38. Johnson, M. L., and Faunt, L. M. (1992) Parameter estimation by least-squares methods, *Methods Enzymol. 210*, 1−37.
39. Christensen, R. L., Goyette, M., Gallagher, L., Duncan, J., DeCoster, B., Lugtenburg, J., Jansen, F. J., and van der Hoef, I. (1999) S_1 and S_2 states of apo- and diapocarotenes, *J. Phys. Chem. A 103*, 2399−2407.
40. Polívka, T., Pullerits, T., Frank, H. A., Cogdell, R. J., and Sundström, V. (2004) Ultrafast formation of a carotenoid radical in LH2 antenna complexes of purple bacteria, *J. Phys. Chem. B 108*, 15398−15407.
41. Schlücker, S., Szeghalmi, A., Schmitt, M., Popp, J., and Kiefer, W. (2003) Density functional and vibrational spectroscopic analysis of β-carotene, *J. Raman Spectrosc. 34*, 413−419.
42. Billsten, H. H., Zigmantas, D., Sundström, V., and Polívka, T. (2002) Dynamics of vibrational relaxation in the S_1 state of carotenoids having 11 conjugated C═C bonds, *Chem. Phys. Lett. 355*, 465−470.
43. de Weerd, F. L., van Stokkum, I. H. M., and van Grondelle, R. (2002) Subpicosecond dynamics in the excited-state absorption of all-trans β-carotene, *Chem. Phys. Lett. 354*, 38−43.
44. Larsen, D. S., Papagiannakis, E., van Stokkum, I. H. M., Vengris, M., Kennis, J. T. M., and van Grondelle, R. (2003) Excited-state dynamics of β-carotene explored with dispersed multi-pulse transient absorption, *Chem. Phys. Lett. 381*, 733−742.
45. Diversé-Pierluissi, M., and Krogmann, D. W. (1988) A zeaxanthin protein from *Anacystis nidulans*, *Biochim. Biophys. Acta 933*, 372−377.
46. Ilagan, R. P., Chapp, T. W., Christensen, R. L., Gibson, G. N., Pascher, T., Polívka, T., and Frank, H. A. (2005) Femtosecond time-resolved absorption spectroscopy of astaxanthin in solution and in β-crustacyanin, *J. Phys. Chem. B*, in press.
47. Zigmantas, D., Polívka, T., Hiller, R. G., Yartsev, A., and Sundström, V. (2001) Spectroscopic and dynamic properties of the peridinin lowest singlet excited states, *J. Phys. Chem. A 105*, 10296−10306.
48. Groot, M. L., van Wilderen, L. J. G. W., Larsen, D. S., van der Horst, M. A., van Stokkum, I. H. M., Hellingwerf, K. J., and van Grondelle, R. (2003) Initial steps of signal generation in photoactive yellow protein revealed with femtosecond mid-infrared spectroscopy, *Biochemistry 42*, 10054−10059.
49. Jurgens, U. J., and Mantele, W. (1991) Orientation of carotenoids in the outer membrane of *Synechocystis* PCC-6714 (cyanobacteria), *Biochim. Biophys. Acta 1067*, 208−212.

BI047473T